Clim Dyn (2015) 44:2825–2837
DOI 10.1007/s00382-014-2422-z

Global eastward propagation signals associated with the 4–5-year ENSO cycle

S.-Y. Simon Wang · Xianan Jiang · Boniface Fosu

Received: 20 January 2014 / Accepted: 17 November 2014 / Published online: 28 November 2014

Abstract Longitude-time evolution of sea surface temperature anomalies (SSTA) reveals a slow southeastward propagation from the western North Pacific (WNP) around 20°N to the Niño-3.4 region in the equatorial Central Pacific. The propagation is manifested as a narrow, southwest-northeast oriented SSTA band across the subtropical North Pacific, and its journey takes about 2–3 years. The propagating SSTA appears to engage the initiation of the El Niño–Southern Oscillation (ENSO). The anomalies of surface winds, sea level pressure, outgoing longwave radiation, and velocity potential all exhibit a concurrent and distinct eastward propagation, one that appears to be circumglobal and is coupled with the predominant 4–5 year frequency of the ENSO cycle. It is suggested that the previously found warming/cooling in the Indian Ocean induced by El Niño/La Niña, the progressive SSTA and wind anomalies across the Indian Ocean towards the WNP, and the predominant 4–5-year frequency of the North Pacific Oscillation collectively contribute to the reported SSTA propagation . The findings implicate that monitoring the SSTA propagation from the WNP towards the tropical central Pacific could be useful in tracking the ENSO development.

Keywords ENSO cycle · SST propagation · Precursor · Prediction · WNP

1 Introduction

Long-lead prediction of El Niño–Southern Oscillation (ENSO) relies critically upon the identification and tracking of "precursor patterns" in the sea surface temperature anomalies (SSTA) and winds that precede an ENSO event. (Penland and Sardeshmukh 1995) have found an optimal SSTA structure across the North Pacific Ocean during the northern spring. Since then, three primary (but not exclusive) ENSO precursors have been identified in the Northern Hemisphere—these are outlined in Fig. 1a from west to east: (1) the northern/tropical Indian Ocean (IndO) that features prominent surface wind and SSTA signals preceding an ENSO event as far back as 15 months (Clarke and Van Gorder 2003; Izumo et al. 2010); (2) the analogous western North Pacific (WNP) pattern of SSTA located in the east of Taiwan and south of Japan that forms (with opposite signed SSTA) 1 year before a full-fledged ENSO event (Wang et al. 2012, 2013); (3) the Pacific Meridional Mode (PMM) over the eastern half of the North Pacific (Chang et al. 2007; Chiang and Vimont 2004) in which the atmospheric variability during the preceding spring influences SSTA across the equatorial Pacific and then triggers ENSO; this is known as the Seasonal Footprinting Mechanism (Alexander et al. 2010; Anderson 2003; Vimont et al. 2001, 2003).

Another notable feature associated with ENSO development is the seasonally phase-locked propagation of wind

Electronic supplementary material The online version of this article (doi:10.1007/s00382-014-2422-z) contains supplementary material, which is available to authorized users.

S.-Y. Simon Wang (✉)
Utah Climate Center, Utah State University, Logan, UT, USA
e-mail: simon.wang@usu.edu

S.-Y. Simon Wang · B. Fosu
Climate Sciences Program, Utah State University, Logan, UT, USA

X. Jiang
Joint Institute for Regional Earth System Science and Engineering, UCLA, Los Angeles, CA, USA

and SSTA signals, which allows tracking of the progression of an ENSO event. The phase-locked propagating signal first appears in the eastern Indian Ocean in the middle of the year before an El Niño and then moves eastward, reaching the western Pacific during the beginning of the El Niño year and then amplifying in the central equatorial Pacific (Gutzler and Harrison 1987; Meehl 1987); similar but opposite-signed propagating signals also appear during La Niña. Such propagation may connect the aforementioned three ENSO precursors, as is illustrated by their seasonal cross-correlations with the wintertime (December–February; DJF) Niño-3.4 index in the following year (Fig. 1b): Peak correlations occur for six seasons in IndO prior to an ENSO event, 4–5 seasons in WNP (sign reversed; explained later) and three seasons in PMM.

Most previous studies that focus on the propagating signature of the ENSO evolution stressed either (a) the favorable wind and SSTA forcing up to 1 year in advance, or (b) the emerging SST signals over the Indian/Atlantic Ocean after the ENSO decay. In this study, we present observational evidence that the propagating SSTA signal following the IndO → WNP → PMM route as noted in Fig. 1 is prolonged, systematic and could be trackable. In particular, while the transition of opposite-sign SSTA from WNP to Niño-3.4 amounts to 1 year (Wang et al. 2012, 2013), we will show that the same-signed SSTA slowly propagates from WNP to Niño-3.4 over a duration of 2–3 years and appears to connect with the initiation of an ENSO event. Thus, tracking the persistent propagation of SSTA from WNP to Niño-3.4 could be useful in monitoring and potentially predicting ENSO at long lead-time.

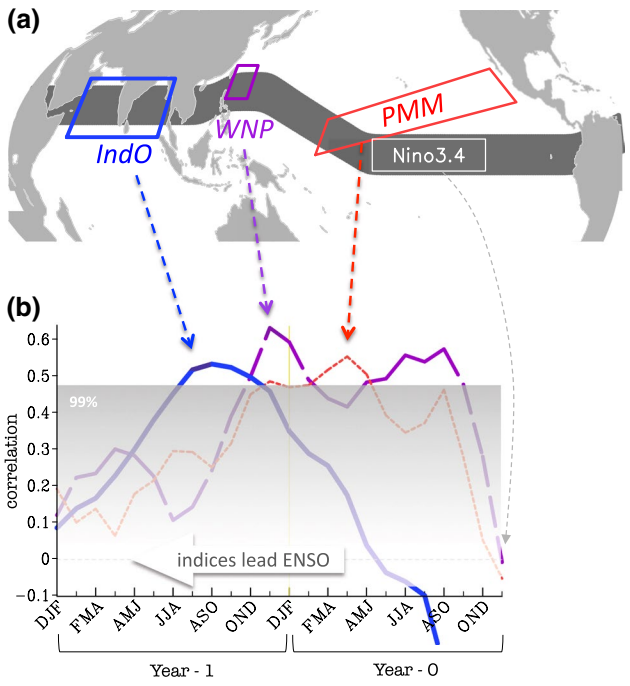

Fig. 1 **a** Domains of common ENSO precursors outlined for the Indian Ocean mode (IndO), the Western North Pacific mode (WNP; sign reversed), the Pacific Meridional Mode (PMM) and the Niño-3.4 region. The *dark strip* that runs across these three domains indicate the section from which the longitude-time evolution in Fig. 2 was constructed. **b** Cross-correlations of the DJF Niño-3.4 index with the 3-month mean IndO (*blue*), WNP (*purple*; sign reversed), and PMM (*red*) over the preceding 2 years. *Shaded area* indicates the 99 % confidence interval

2 Data

The following data were utilized: (1) the NOAA Extended Reconstructed SST Version 3b (Smith et al. 2008) beginning in 1854, and (2) the NCEP/NCAR Global Reanalysis of tropospheric and surface data that begin in 1948 (Kalnay et al. 1996), (3) the Niño-3.4 index provided by the Climate Prediction Center (http://www.cpc.ncep.noaa.gov/data/indices/) and the PMM index developed and provided by (Chiang and Vimont 2004) (http://sunrise.aos.wisc.edu/~dvimont/MModes/Data/), and (4) Ocean temperature and current data were obtained from the NCEP Global Ocean Data Assimilation System at the resolution of 0.333° latitude × 1.0° longitude with the vertical levels ranging from 5 to 4,479 m depth, starting January 1980 (Behringer et al. 1998).

3 Results

3.1 The propagating signal

We constructed the longitude-time evolution of monthly SSTA from a 10°-latitude average along the route displayed in Fig. 1a—i.e. across the northern Indian Ocean, the subtropical WNP, and the equatorial Eastern Pacific (and then up north about 17.5°N till 30°W in connecting the North Atlantic; not shown) from 1854 to 2013, and this is shown in Fig. 2. The SSTA displayed here were detrended and bandpass-filtered within 3–6 years based upon the predominant ENSO frequency (discussed later); non-filtered SSTA are shown in the supplementary Figure. For the filtering we used the Hamming-windowed bandpass method that was developed to preserve the edges of the filtered time series (Iacobucci and Noullez 2005). Beginning in 1870, a systematic propagating pattern of SSTA has emerged between 100°E and 160°W, linking warm (cold) water in the WNP to the development of El Niño (La Niña) in the central equatorial Pacific, for a duration of about 2–3 years. Also noteworthy after 2010 is the connection of the SSTA propagation towards the ongoing (2014–2015) development of El Nino. Prior to 1880, the weak and disorganized SSTA pattern is likely due to questionable data quality; while poor

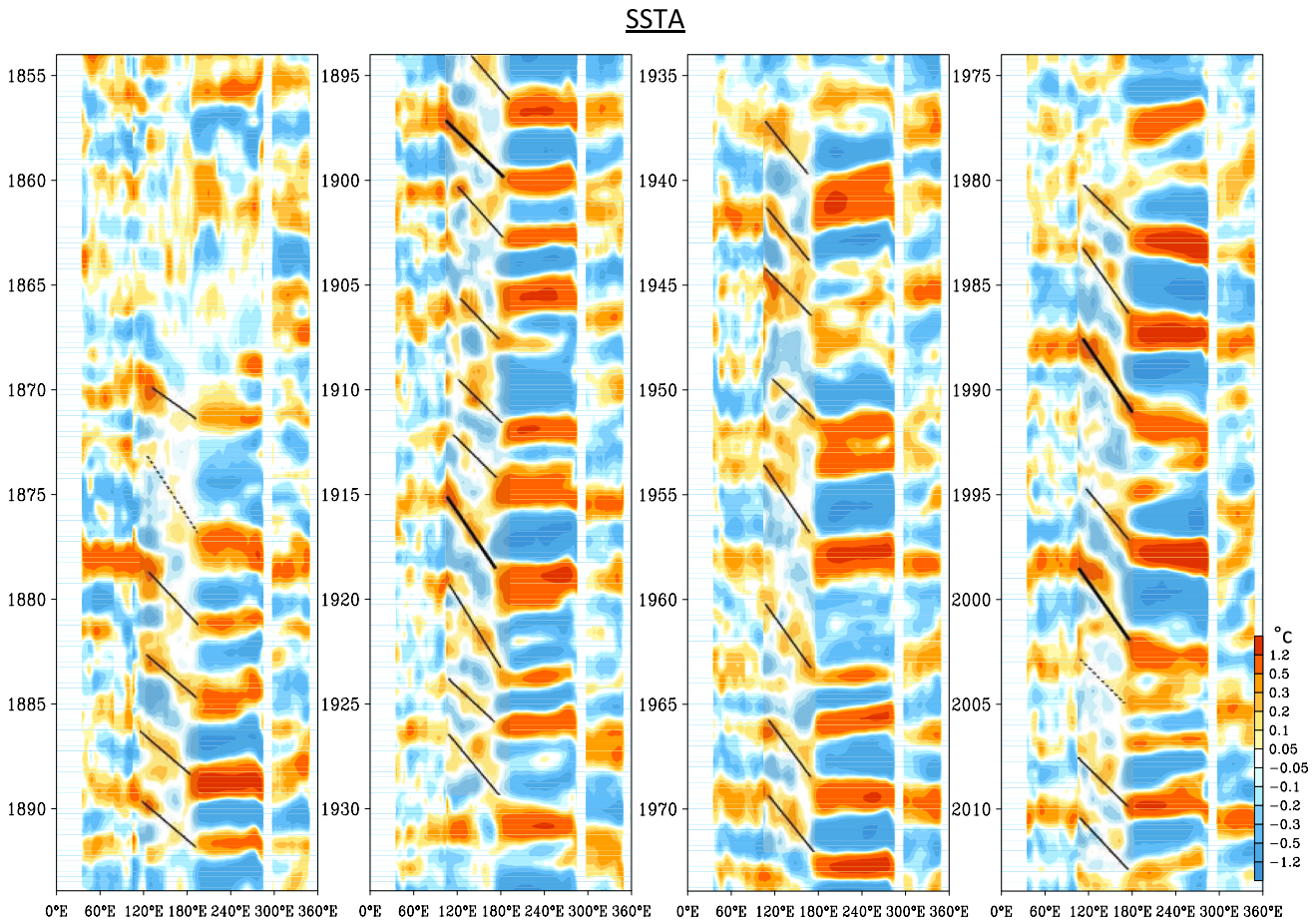

Fig. 2 Longitude-time section of bandpassed SSTA since 1854 across the 10°-latitudinal belt indicated in Fig. 1a. The SSTA were detrended and filtered by a 3–6 year HW bandpass. *Black lines* between 120°E and 180° were subjectively added to illustrate the eastward propagation of SSTA; *dashed lines* represent weak cases and *thick solid lines* represent strong ones

data coverage before World War II over the north Indian Ocean (Chowdary et al. 2012) might also disturb signals in Fig. 2.

Overall, Fig. 2 shows that (1) the northern Indian Ocean warming/cooling connects to the WNP warming/cooling within a season or two, (2) the positive/negative SSTA then propagate at a much slower pace towards the central equatorial Pacific, then (3) merge into a new phase of El Niño/La Niña after 2–3 years, and (4) the positive/negative SSTA moves into the tropical Atlantic after a season or two. To substantiate this slow SSTA propagation, black lines were subjectively added over positive SSTA strips between 120°E and 180°. Some recent El Niño events are apparently linked to the propagating SSTA signal, such as 1982/1983, 1987/1988, 1991/1992, 1997/1998 and 2009/2010. The eastward movement of negative SSTA is similarly evident and appears to connect with La Niña events, such as 1984/1985, 1988/1989, 1998/1999 and 2010/2011. Exception does exist, however, such as the years leading up to the 1997/1998 El Niño, i.e. the Indian Ocean warming was much weaker during 1995 in comparison to adjacent El Niño events. The 1997/1998 El Niño, being the strongest on record, has been extensively studied and multiple factors have been suggested: e.g., westerly wind bursts (Vialard et al. 2001) commonly associated with the Madden–Julian oscillation (Takayabu et al. 1999) were an apparent cause in 1997, as well as other theories invoked to account for the irregularity of the ENSO cycle (McPhaden 1999a).

Confusion of thought needs to be addressed here regarding the previously reported 1-year lag between WNP and ENSO and its distinction from the 2–3-year propagation as shown in Fig. 2. The so-called WNP pattern defined by (Wang et al. 2012) consists of an opposite-signed SSTA dipole located off southeastern Asia and in the western tropical Pacific, which is accompanied by equatorial winds that influence the level of oceanic Kelvin wave activity, which then precedes ENSO events. Though the WNP index can be constructed by using a Maximum Covariance Analysis between SSTA and surface wind anomalies over the WNP region, it could also be simply produced by

averaging de-trended SSTA over 122°–132°E to 18°–28°N centered at the upstream Kuroshio Current (Fig. 1a purple box). Therefore, it is the negative (positive) SSTA in the WNP domain that leads warm (cold) ENSO by 1 year—hence the sign-reversed correlation in Fig. 1b. What is shown in Fig. 2 indicates a much slower propagation of the same-sign SSTA from WNP to central equatorial Pacific, a previously undocumented feature that is examined herein.

Noteworthy of the SST propagations in Fig. 2 is the sign flip between the Indian Ocean and the eastern equatorial Pacific, halfway through an ENSO event. This feature reflects the marked correlation reversal between IndO and ENSO (Fig. 1b) and echoes the remote impacts of ENSO on the Indian Ocean SSTA, known to occur at the El Nino developing summers (Klein et al. 1999; Yang et al. 2007; Yu et al. 2002). (Xie et al. 2009), among others, have suggested that both the tropical Indian Ocean SSTA and tropical tropospheric temperature increase in spring after El Niño of the previous winter, and the warming persists through the summer even after El Niño has dissipated. (Izumo et al. 2010) found that a negative phase of the Indian Ocean SSTA provides an effective predictor of El Niño 14 months before its peak, and vice versa for La Niña. According to Fig. 2, the remnant warm (cold) IndO appears during the mature phase of a warm (cold) ENSO event, and then persists for a year or two while propagating eastward. During the propagation (when positive SSTA is still located around 140°E), a cold ENSO event occurs in the eastern Pacific. This feature echoes the observations by (Du et al. 2011), (Xie et al. 2009) that the termination of El Niño could help develop La Niña soon after. However, the propagation as shown in Fig. 2 is not zonal, but rather tilts northward through the WNP region and then southward towards the central-eastern tropical Pacific. Consequently, a strictly zonal cross-section of SSTA, such as that along the equator plotted in (Xie et al. 2009; their Fig. 5), could not depict the southeastward, trans-Western Pacific SSTA propagation. Furthermore, the connection between major El Niño/La Niña and the subsequent appearance of positive/negative SSTA in the tropical Atlantic has been noted by (Enfield and Mayer 1997), who found that Atlantic warming occurs 4–5 months after the mature phases of El Niño. On the other hand, (Rodríguez-Fonseca et al. 2009) suggested that warm Atlantic SSTA (Atlantic Niño) could induce Pacific La Niña through the strengthening of Walker Circulation.

3.2 Robustness of the signal

To examine the significance of the propagating SSTA as shown in Fig. 2, we conducted a spectral coherence analysis between the indices of winter mean WNP and Niño-3.4 (unfiltered data), using the multi-taper method of (Mann and Park 1996) for the period of 1958–2013 (chosen for increased observations after the International Geophysical Year). As shown in Fig. 3a, a high degree of coherence between WNP and Niño-3.4 appears in the 4–5 year frequency band and it is significant at the 99 % level; this 4.5 year spectral peak was the basis for the bandpass filtering of 3–6 years used for the longitude-time plots in Fig. 2 and later analyses. The phase difference between WNP and Niño-3.4 is −60°, indicating that either the WNP leads the opposite-sign Niño-3.4 by about a year (as in Wang et al. 2012) or the WNP leads the same-sign Niño-3.4 by about 3 years; i.e. a 300° phase shift over a 4.5 year cycle.

To delineate the SSTA coherence pattern, we plotted in Fig. 3b the geographical distribution of the spectral coherence. This analysis proceeds along the following lines: first, the spectral coherence was computed between the DJF mean WNP and SSTA everywhere so that the spatial distribution of their coherence and phase could be constructed at each grid point. Since our focus was on the 4–5 year time scale, only the maximum coherence (amplitude) within that frequency band and its corresponding phase are displayed—i.e. vector length shows coherence amplitude and vector direction indicates phase difference. Significant coherence amplitudes were observed across the Western Pacific with an overall

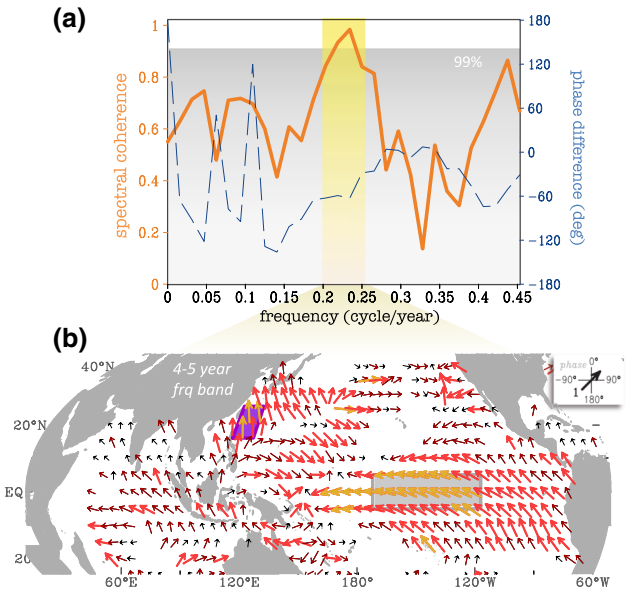

Fig. 3 **a** MTM spectral coherence analysis between the DJF-mean WNP and Niño-3.4 indices (1958–2012) showing the coherence amplitude (*orange line*) and phase difference (*blue broken line*). *Shaded area* indicates the 99 % confidence interval. The significant frequency of 4–5 years is *highlighted*. **b** Maximum coherence amplitudes (*vector length*) and corresponding phases (*vector direction*) between WNP and SSTA within the 4–5 year frequency band. Coherence amplitudes above the 90 % confidence interval are shown in *dark red* (*thin*); 95 % in *red*; 99 % in *golden*. The phase direction is explained at the *top right corner*

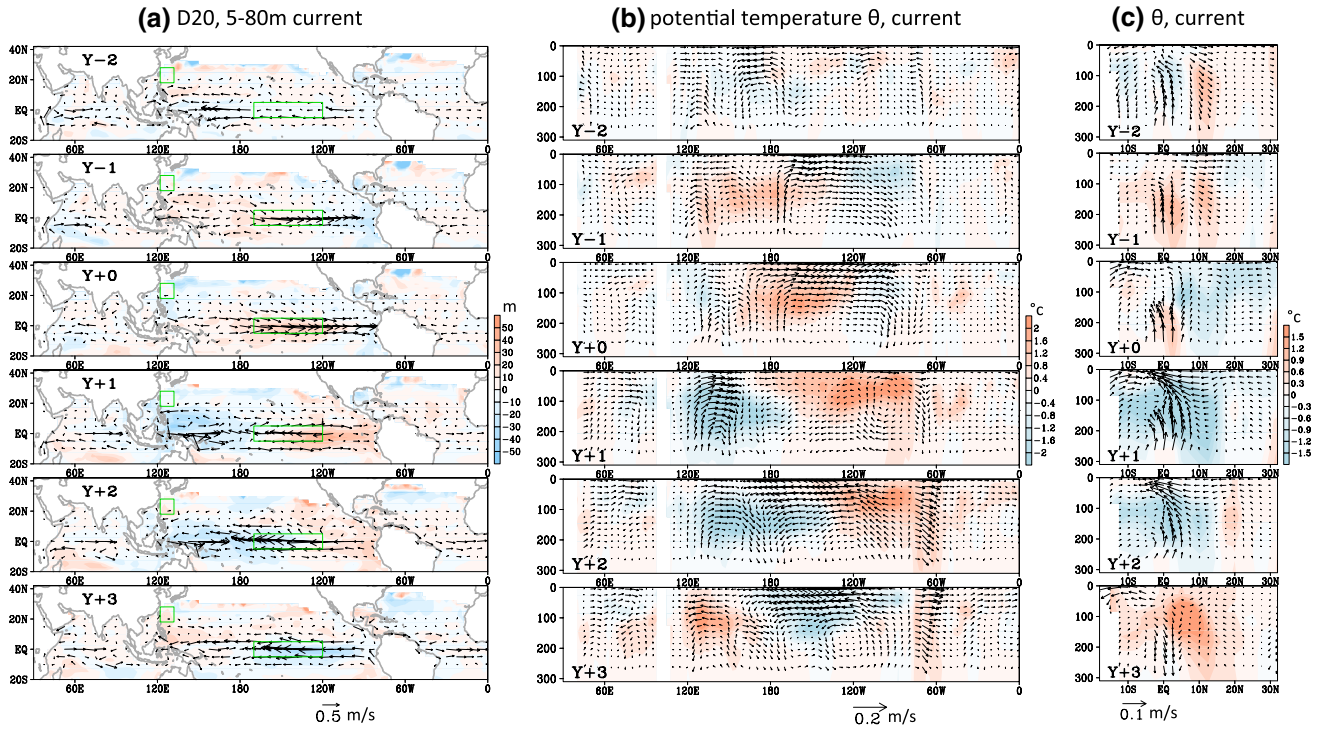

Fig. 4 For the DJF season, (**a**) lagged regressions of bandpassed 20 °C isotherm depth (D20) and averaged currents at the 5–80 m depth (*vectors*) with the sign-reversed, standardized WNP index for six lags, from Y − 2 to Y + 3, with Y + 1 representing the El Nino conditions. **b** and **c** Similar with (**a**) except for the vertical sections of potential temperature and ocean currents across 5°N and 130°E, respectively. The WNP index was standardized between −1 and 1 and so, the regression coefficients of each variable retain their native unit. The analysis period is 1981–2013; significance levels are not shown to simplify the illustration

1.5-year phase lag in the subtropics (100°E–160°W) and a 3-year phase lag in the Niño-3.4 region, relative to WNP. Moderate coherence in the Indian Ocean reveals a 0.5-year lead to WNP. The combination of these phase differences of spectral coherence provides statistical evidence of the SSTA propagation within the significant 4–5 year frequency.

3.3 Oceanic features

A 4–5-year oscillation shared by the WNP and Niño-3.4 indices echoes the well known low-frequency mode (3–7 years) of the ENSO cycle, which is partly due to the slow oceanic dynamic adjustment of equatorial heat content (Bejarano and Jin 2008; White et al. 2003). To examine the association of this heat content adjustment with the WNP, we computed the lagged regressions for the northern winter 20 °C isotherm depth (D20) and the 5–80 m averaged currents with the WNP index for six lags from 2 years before to 3 years after the WNP (Y − 2 to Y + 3) (note: here the WNP index was reversed in sign). The results are plotted in Fig. 4a with bandpass filtered data. A steady eastward propagation of D20 anomalies was observed in the tropics moving from the western edge of the Pacific Ocean to the eastern basin. The upper-layer currents alternate between predominantly easterly to westerly flows, exhibiting basin-wide easterly (westerly) currents 1 year before (after) the El Niño condition. This slow alternations of D20 and currents reflect the recharge oscillator theory concerning thermocline and zonal advection feedbacks within the equatorial Pacific (Jin and An 1999), which cause a delayed response on SSTA (White et al. 2003). Similarly, Fig. 4b shows the vertical sections of potential temperature anomalies and zonal-vertical currents across 5°N regressed with WNP. From Y − 2 to Y + 2, warm upper-level water is observed to migrate from the northern Indian Ocean towards the eastern Pacific, and then connects with the tropical Atlantic (though wind forcing; explained later). Also noteworthy is the appearance of subsurface warm water in the western tropical Pacific (Y − 1), 2 years prior to El-Niño (Y + 1), or 1 year before the WNP (Y + 0). Analyzing the 1997/98 El Niño, (McPhaden 1999b) has also observed a prolonged propagation of D20 and zonal currents (his Fig. 2).

To examine the north-south movement, Fig. 4c shows the vertical sections of potential temperature and meridional currents at 130°E, across the WNP region. There is an equatorward propagation of cold water beginning at about 20°N from Y − 1 to Y + 1. During Y + 0, surface convergence and downwelling around 20°N indicate the WNP's association

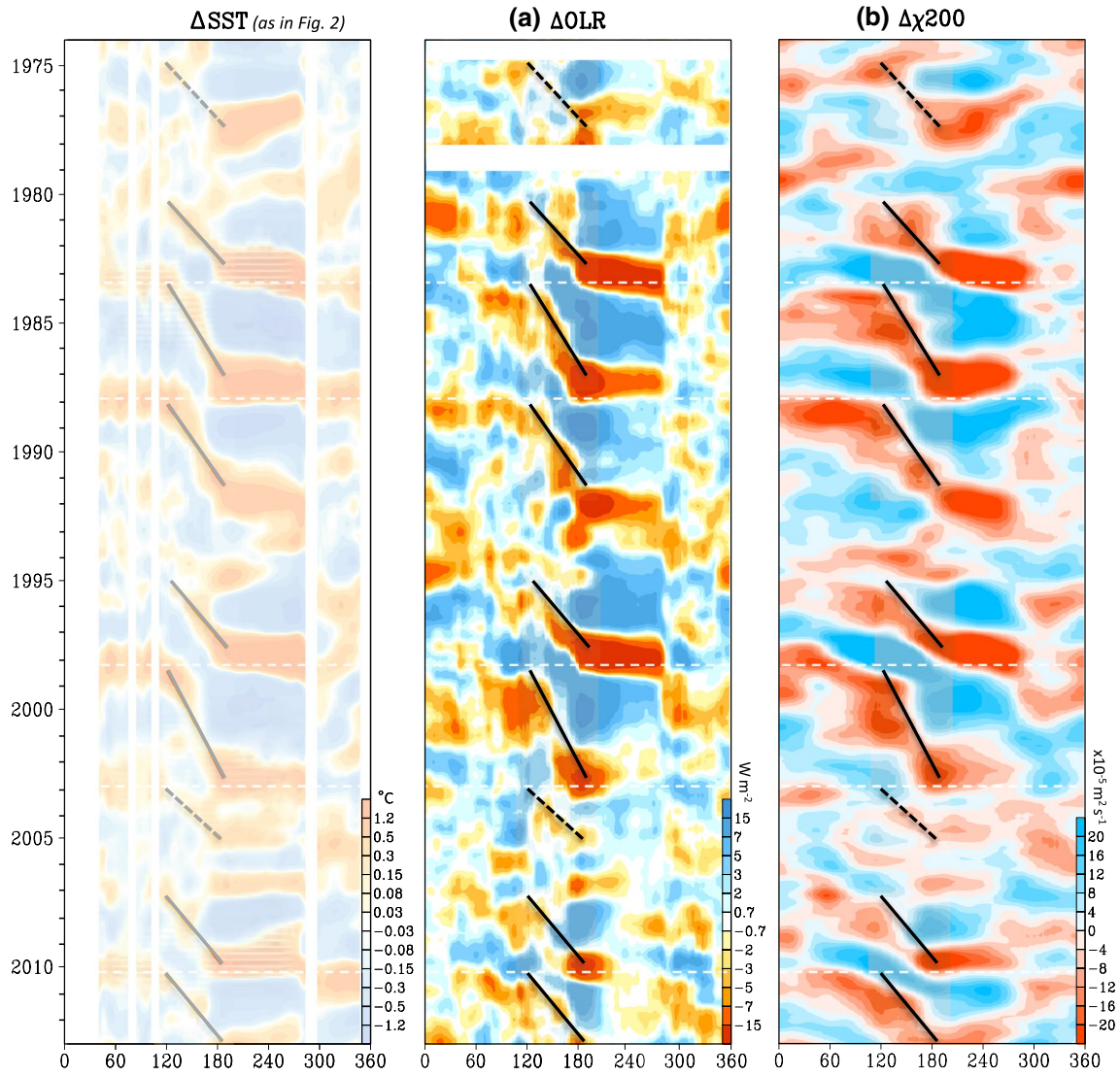

Fig. 5 Same as Fig. 2 after 1974 (which was repeated in the *left column* for ease of comparison) except for (**a**) OLR and (**b**) 200-hPa velocity potential (χ) anomalies across the 10°-latitudinal band as outlined in Fig. 1a. All variables were detrended and filtered with 3–6 years. *Black lines* between 120°E and 180° were subjectively added in accordance with the SSTA propagation, and were repeated onto OLR and χ at the same position as reference. *White dashed lines* indicate major Indian Ocean warming events

with cold air advection acting to cool the surface water. This cooling effect of downwelling is in contrast with the upwelling cooling that is most common in the tropics (as is the case from Y + 0 to Y + 2 around 10°N). (Wang et al. 2012) have shown that surface winds associated with the anomalous East Asian anticyclone could feedback onto the negative SSTA in the WNP by producing cold air advection over the Kuroshio Current and further cooling the SSTs. Because the WNP domain is situated in the strong east–west SST gradients (Fig. 1a), it is sensitive to temperature advection effects associated with the winter monsoon there. Likewise, a cyclonic anomaly (i.e. weaker winter monsoon) may result in warm air advection towards the East Asian coastal seas and consequently enhance positive SSTA (as in warm WNP cases).

3.4 Atmospheric coupling

Following the longitudinal-time diagrams of SSTA in Fig. 2, we next computed the OLR anomalies to examine the response in tropical convection. The OLR propagation pattern, as shown in Fig. 5a, is synchronized with the SSTA propagation but exhibits a phase shift: i.e. negative (positive) OLR trails positive (negative) SSTA until 160°W. Over the Indian Ocean, increased (decreased) convective activity occurs 6 months after the emergence of warm (cool) SSTA. This feature reflects the previous observations (Klein et al. 1999; Meyers et al. 2007; Xie et al. 2002) that the Indian Ocean basin warming (cooling) could be induced by the atmospheric forcing of El Niño (La Niña) through the

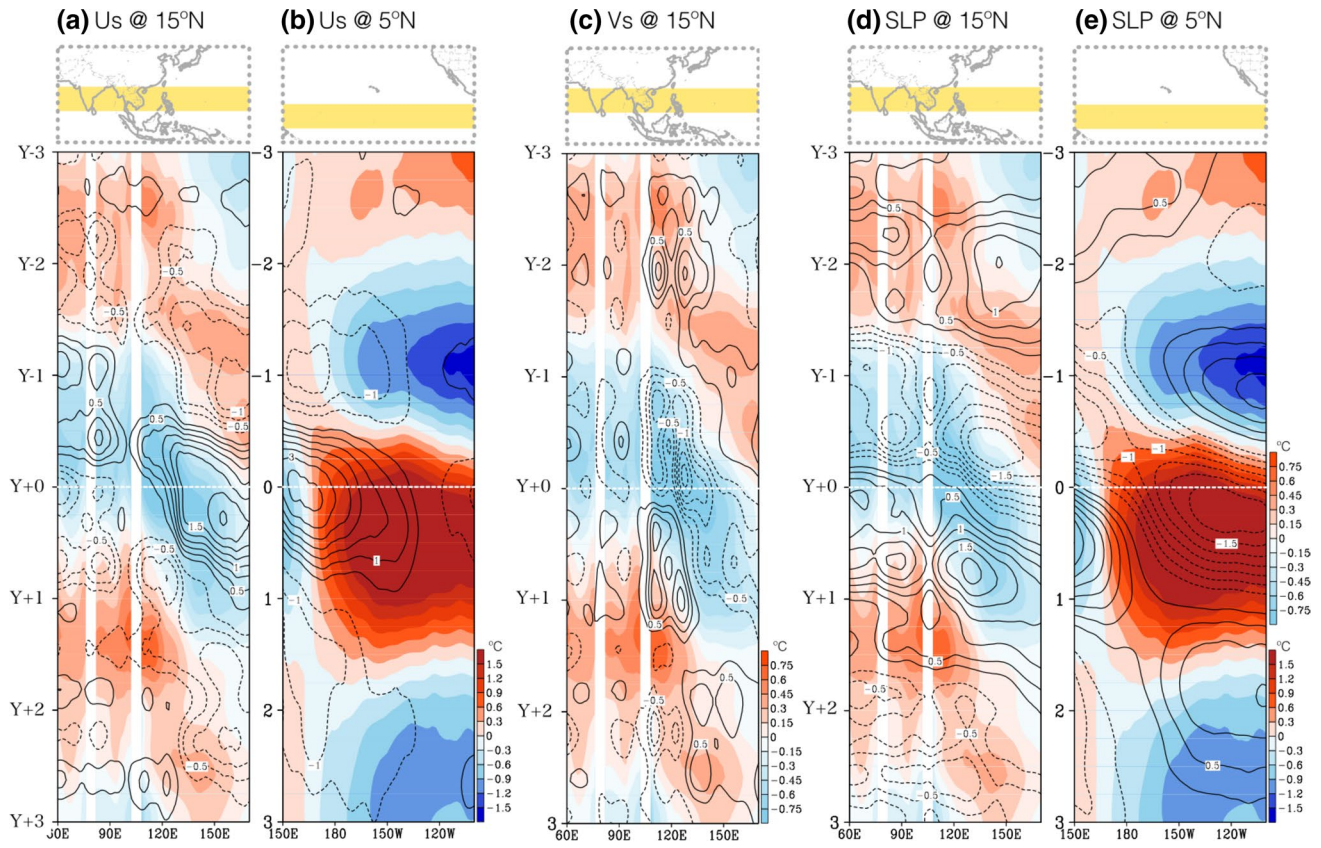

Fig. 6 Longitude-time sections of regressed SSTA (*shading*) and surface zonal winds (Us; *contours*) with the sign-reversed, standardized WNP index across (**a**) 15°N over the Indian Ocean-western Pacific and (**b**) 5°N over the eastern Pacific. **c** Same as (**a**) but for meridional surface winds (Vs; *contours*). **d** and **e** Same as (**a**, **b**) but overlaid with SLP (*contours*). The situation at Y + 1 reflects El Niño; Y + 0 reflects negative WNP. All the variables were detrended and filtered by a 3–6 year HW bandpass and averaged within the 15° latitudinal band, which is *highlighted in the map atop each panel*. The analysis period is 1958–2013

modulation of heat flux (i.e. "tropical atmospheric bridge"), that is, eastern Pacific warming suppress convection in the Indian Ocean initially, causing the SST to warm and, subsequently, enhance convection in the Indian Ocean when El Niño starts to decay. Here, an additional feature not revealed before is the concurrence of OLR anomalies over the northern Indian Ocean and North Atlantic (0°–60°E); in fact, in some cases the OLR anomalies propagate from the Atlantic into the Indian Ocean for a duration of 3–6 months. This OLR feature suggests certain atmospheric processes that help link the Pacific SSTA to the Atlantic SSTA. Indeed, Fig. 5b shows that the 200-hPa velocity potential (χ) anomalies also propagate eastward with respect to SSTA and OLR. The propagation of upper-level divergence (convergence) corresponds well with enhanced (suppressed) convection. The χ propagation also trails SSTA until it reaches 160°W, at which point the χ circulation would be largely influenced by (or coupled with) the matured El Niño/La Niña phases.

To summarize these propagating features, we computed the one-point lagged regression for SSTA, surface winds, and sea level pressure (SLP) with the WNP index. The sign of WNP was reversed here to portray El Niño development in the following year, and the regressed variables were bandpass filtered following Fig. 2. The time lags involved are 3 years prior to (Y − 3) and 3 years after (Y + 3) the WNP; i.e. Y + 0 represents the WNP situation and Y + 1 represents the El Niño conditions. Figure 6a shows the longitude-time progressions of SSTA and surface zonal wind (Us) across 10–20°N over the western Pacific (the domain is shown in the top map); Fig. 6b shows the progressions across EQ-10°N over the eastern Pacific. The eastward propagation of both SSTA and Us are evident between 100°E and 180°E, with westerly winds leading colder SST (easterlies leading warmer SST) by about a half year while pushing warm water towards the eastern Pacific; this feature is well-known and reflects the wind-evaporation-SST feedback. Figure 6c shows the progression of surface meridional wind (Vs), which also depicts a clear, concurrent propagation with SSTA. The cooling effect of the northerly winds on the ocean surface is evident. This cooling effect echoes the finding of (Wang et al. 2012) that stronger-than-normal East Asian winter monsoons

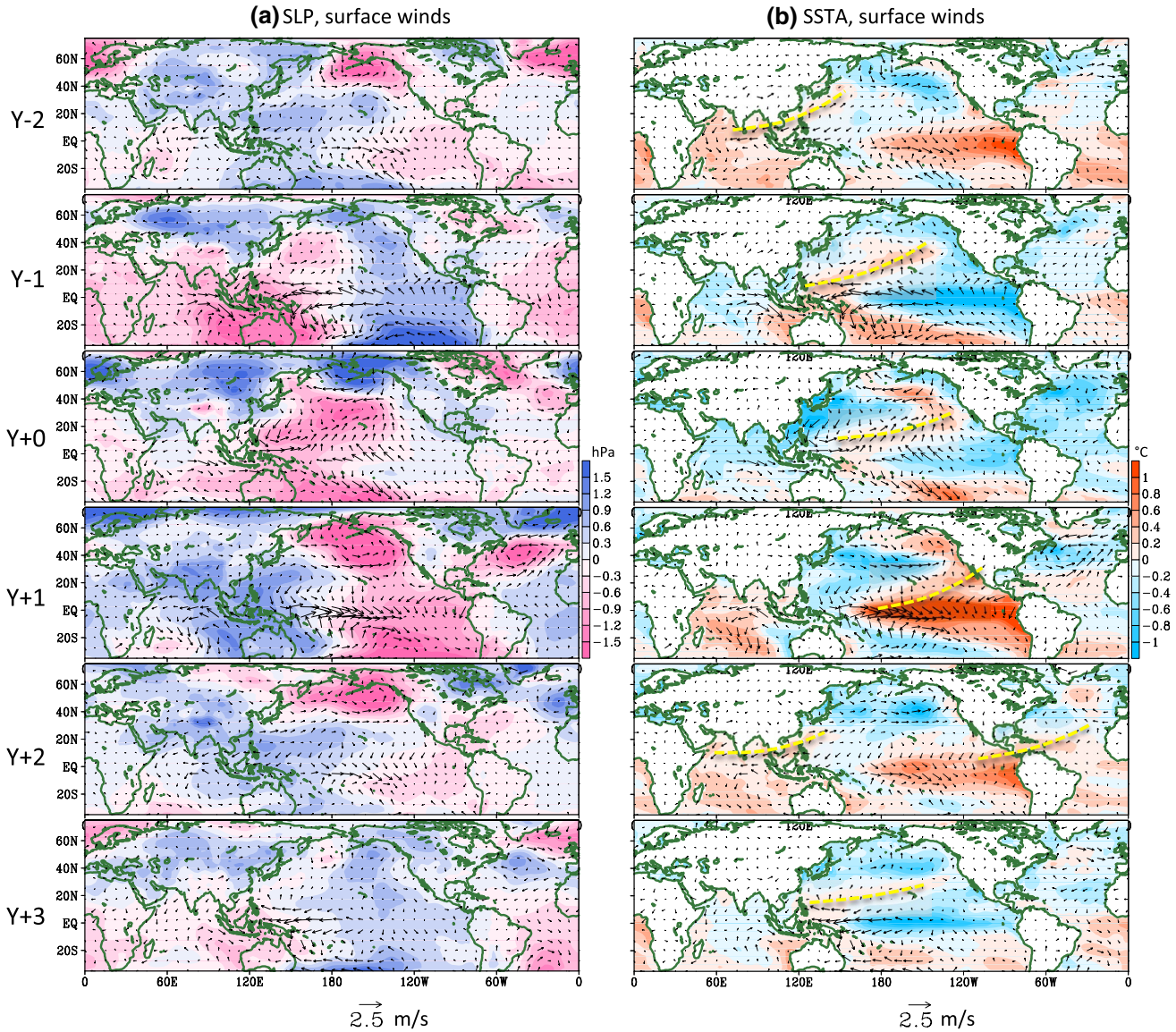

Fig. 7 Horizontal maps of surface winds (*vectors*) overlaid with (**a**) SLP and (**b**) SSTA (*shadings*) regressed with the sign-reversed, standardized WNP index for six lags from Y − 2 to Y + 3. The situation at Y + 1 reflects El Niño; Y + 0 reflects negative WNP. Significance tests are not shown, but in general |SLP| greater than 0.6 and wind speed larger than 1.0 are significant at the 95 % confidence level. The analysis period is 1948–2013

act to cool SST in the WNP region (ref., Fig. 4c). Beginning in Y + 0, the cooled water off the East Asian coast then propagates towards central equatorial Pacific and, as Fig. 6b shows, later merges into a La Niña. Next, we show the regression pattern of SLP in Fig. 6d, e, which reveals a robust propagation with low-pressure anomalies leading negative SSTA up to the central Pacific, prior to the development of an El Niño. Of note, the propagation of SLP anomalies from the northern Indian Ocean to the Eastern Pacific takes 3 years between Y − 2 and Y + 1. While SLP appears to force the SSTA from Y − 1 to Y + 0 (i.e. low pressure with negative SSTA), the mature phase of ENSO in the eastern Pacific at Y + 1 reverses the SLP response (i.e. low pressure with positive SSTA), though the SLP anomaly continues to migrate eastward across the Atlantic (not shown).

3.5 A global propagation?

To delineate the horizontal patterns with respect to the WNP–ENSO evolution, we plotted in Fig. 7a the SLP and surface wind anomalies regressed with the (sign-reversed) WNP index. A global eastward propagation of SLP and associated wind anomalies is readily visible within the

subtropical zone (between about 30°N and 30°S). In the higher latitudes, however, there is not a discernable propagation across the globe, as the SLP anomalies are largely constrained within the northern ocean basins. Yet, there appears to be an apparent "half-rotation" manifested in the pressure anomalies over the North Pacific, i.e. SLP cell moving from the tropical Western Pacific (Y − 1) towards central-Eastern Pacific (Y + 0) and then up north to the central North Pacific (Y + 1), and dissipates later (Y + 2). At Y + 0, the high-pressure anomalies in Siberia and East Asia indicate the enhanced winter monsoon. Figure 7b shows the same regression maps with SSTA and surface winds, depicting the propagating band of warm water from South/East Asia towards central-Eastern Pacific associated with the southern lobe of the low-pressure anomalies; this SSTA band is indicated by dashed yellow lines. The positive SSTA regenerates after about 4 years along the South/East Asia coasts.

The evolution of the SLP and SST patterns in the North Pacific may resemble the transition from the so-called West Pacific (WP) teleconnection pattern first defined be (Walker and Bliss 1932) and the North Pacific Oscillation (NPO) defined by (Rogers 1981) in Y + 0, to ENSO in Y + 1, to the Pacific North America (PNA) pattern as defined by (Wallace and Gutzler 1981) in Y + 2. The NPO is known to significantly impact the SSTA in the central North Pacific, forcing springtime SSTA to excite a surface wind response that extends deep into the tropical Pacific, triggering the onset of ENSO (Vimont et al. 2003). On the other hand, the transition from ENSO to PNA seems counterintuitive, since ENSO and PNA are known to coexist. However, recent studies (Dickey et al. 2003; Huang et al. 2012; Lin et al. 2002) have indicated that the tropical-polar region linkage and the poleward transport of energy/momentum originated from ENSO forcing can generate PNA-like response a year after ENSO and eventually influences the artic region. Moreover, as was pointed out in (Linkin and Nigam 2008), the WP and NPO were defined differently and, upon further examination of their patterns, it appears that the WP resembles more strongly with the Y − 1 situation as shown in Fig. 7a, while the NPO coincides better with the Y + 0 situation. Therefore, there might be a WP → NPO transition that is reflected in the evolution from Y − 1 to Y + 0. Nevertheless, both WP and NPO produce a "triband anomaly structure" in SSTA that creates surface heat flux anomalies linked with SLP variability in the centered North Pacific (Cayan 1992); this triband SSTA resemble the Y + 0 situation and the PMM paradigm in which the relaxed trade winds can lead to equatorial warming in SST to trigger the onset of El Niño (Chang et al. 2007).

The propagation patterns depicted so far were largely based on regression analyses with the WNP index. To validate the propagation features, we adopted an unfiltered, composite approach by defining four phases of the 4–5-year ENSO cycle based upon the Niño-3.4 index. Both the raw and filtered time series of Niño-3.4 are shown in Fig. 8a. The four phases comprise the uptrend (Phase 1; midpoint between warm and cold), extreme warm (Phase 2), downtrend (Phase 3; midpoint between cold and warm) and extreme cold (Phase 4) phases of the 4–5 year ENSO cycle (the years corresponding to each phase are indicated in Fig. 8a). A composite was then constructed using the non-filtered 850-hPa velocity potential anomalies (χ) during DJF based on these four phases. The result is shown in Fig. 8b and

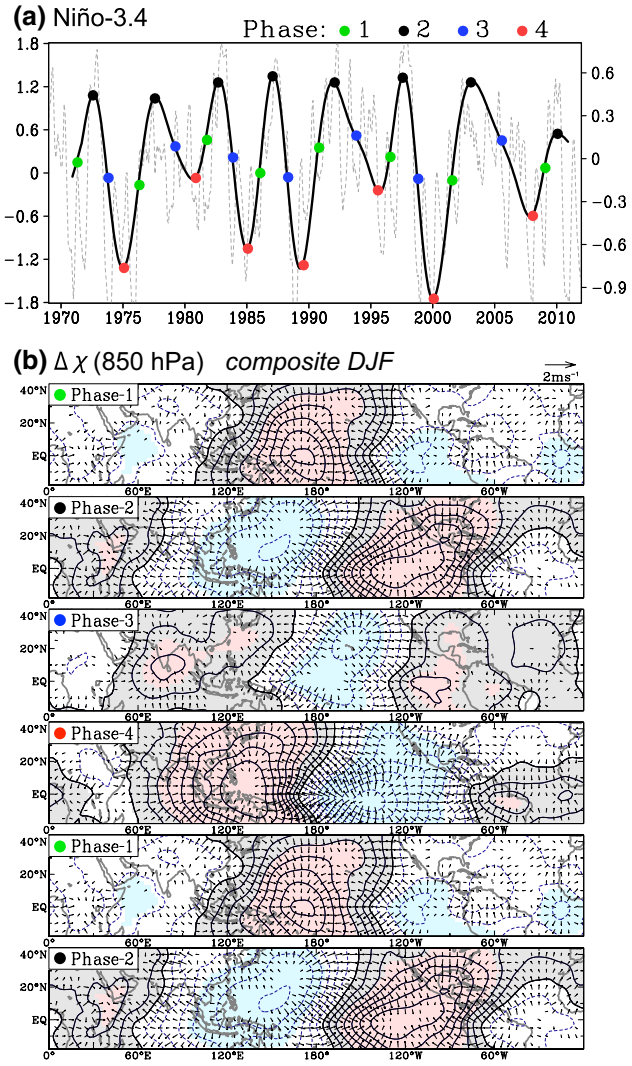

Fig. 8 **a** Monthly unfiltered (*gray dashed line*) and 3–6-year band-pass-filtered (*black thick line*) Niño-3.4 index overlaid with individual phases of the ENSO cycle (*color dots*). Note: the scale for the filtered index is half of that of the raw index. **b** Composite anomalies of the 850-hPa velocity potential during DJF superimposed with the divergent wind vectors (unfiltered, with the zonal mean removed). The contour interval is 1.5×10^5 m^2 s^{-1}. Areas above zero are *shaded* in *gray*; *colored values* are significant at the 95 % confidence interval per *t* test

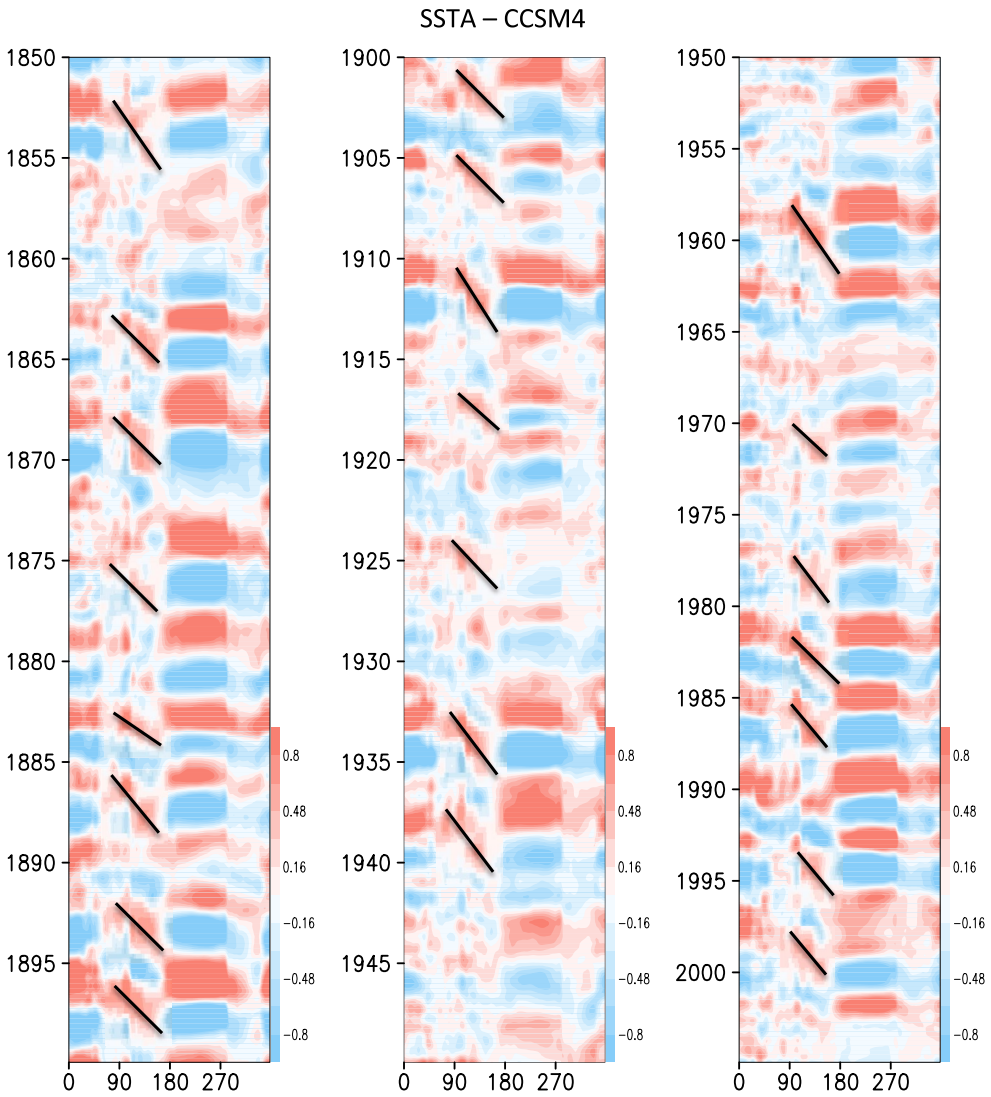

Fig. 9 x–t diagrams of SSTA from the CCSM4 natural-forcing simulations (one member) following Fig. 2, with each column showing 50 years of data. The range of model years is indicated in y-axis and the global range is indicated in x-axis. Unit is °C (note the propagation between 60°E–180 in each column as indicated by black lines)

repeated with phases 1–2 to demonstrate a complete cycle. A striking eastward propagation of the χ circulation stands out as it crosses the globe; this feature corresponds the tropical SLP propagation depicted in Fig. 7. The overall χ circulation consists of a combined zonal wave-1–2 structure with a predominant wave-1 loading, and is tropically confined. In Phase 3, the convergence overlaps with positive SSTA along the coasts of South and East Asia, off the equator, while the divergence over the midlatitude Pacific coincides with divergent winds south of the Gulf of Alaska [similar to that shown in Fig. 7 (Y + 2)]. The χ propagation is more systematic and extensive than the SSTA, of which the propagation is more limited within 100°E–160°W (cf. Fig. 6). These patterns were mirrored in the 200-hPa χ composites (not shown) suggesting an upper-tropospheric response to the SSTA (and OLR) propagation. One other feature also stands out: The convergence/divergence center tends to strengthen while moving across the Indian Ocean and weaken when moving into the Atlantic Ocean, but it subsequently extends over to the northern Indian Ocean, resetting the propagation cycle.

In addition to observed data, we show in Fig. 9 an analysis of the 150-year long Community Climate System Model simulations of SSTA derived from one member of the historical single-forcing (natural-only) experiments as in the CMIP5 (Taylor et al. 2011). Following the SSTA x–t diagram as shown in Fig. 2, each column represents 50 years of monthly data. The eastward propagation of simulated SSTA is readily visible west of the Dateline, though in the simulation, the propagating SSTA do not always connect with an ENSO event. Also noteworthy is the predominant

frequency of 4–6 years revealed from these alternating SSTA patterns. This result is encouraging because (1) it demonstrates that the reported SSTA propagation does exist in a fully coupled environment, and (2) further examination of the physical mechanism is possible given the realistic model simulation. Future work will include sensitivity test of SST in various ocean basins and the role of air-sea coupling.

4 Summary and discussions

What is the physical mechanism that causes the seemingly global propagation of the oceanic and tropospheric circulations embedded in the 4–5 year ENSO cycle? Based upon the empirical analyses presented, we summarize below some plausible explanations for the IndO → WNP → PMM (ENSO) route of the SSTA propagation as noted in Fig. 1.

4.1 IndO → WNP

Previous studies (Barnett 1983; Hendon 2003) have suggested that the seasonal phase-locking mechanism of wind anomalies and SSTA over the eastern Indian Ocean and Indonesia is linked with the phase-locking of equatorial Pacific wind anomalies (Clarke et al. 1998), and this could produce a propagating appearance of the SSTA (Meehl 1987). After El Niño matures, an Indian Ocean warming would likely develop and persist into the next summer (Klein et al. 1999; Xie et al. 2009) while warming near the Philippines and the associated anticyclonic circulation can last until that summer (Wang et al. 2000); these processes have been illustrated in Huang et al. (2010), Chowdary et al. (2011). Moreover, Tourre and White (1997) also found signals of eastward propagating zonal wind stresses and SSTA across the Indian Ocean within the 4–5 year frequency; from there, the signals continue to migrate into the Western Pacific and then merge with ENSO signals along the maritime western boundaries. Although such propagation might be explained by the displacement of the Walker circulation associated with the ENSO evolution (Neelin et al. 1998), the propagating signals in the atmosphere are not confined to the equator and do not resemble any known equatorial waves of the ocean. Furthermore, as one reviewer pointed out, atmospheric Kelvin wave-induced Ekman divergence mechanism (Chowdary et al. 2011; Xie et al. 2010) can link the WNP anticyclone (subtropical gyre) and Indian Ocean SST warming—i.e. during summer following the peak phase of El Nino, surface wind anomalies over the southwestern flank of the WNP anticyclone oppose the mean winds and cause warming in the WNP region.

4.2 WNP → PMM (ENSO)

One pathway that might establish the SSTA's and surface wind's coupling with the 4–5 year ENSO cycle is the speculated WP → NPO evolution. The WP influences the Asian coastal waters and is known to affect the winter monsoon, and the resultant SSTA can be reinforced by the strengthened East Asian winter monsoon during the WNP a year later. Though the WNP is related to the larger-scale NPO (i.e. as part of the NPO's western feature), its influence on ENSO takes place through initiating and sustaining the anomalies of oceanic Kelvin waves in the tropics (Wang et al. 2012); this is different from the seasonal footprinting mechanism acting on the subtropical Eastern Pacific. Because the NPO features a predominant 4–5 year frequency (Wang et al. 2007), coincident with the leading frequency of WNP and its spectral coherence with Niño-3.4, it is possible that the broad North Pacific pressure variability evolves around the WP → NPO → ENSO → PNA sequence and this regulates the lower (interannual) frequency of the ENSO cycle. Theoretical and modeling studies also suggested that the 4–5-year frequency of ENSO is generated through atmospheric processes and air-sea interactions (Clarke 2008). Bottom line, currently there is not a widely accepted theory for the eastward propagation of SSTA from the WNP leading up to ENSO initiation, and none for the pan-global eastward propagation at the 4–5-year frequency. Attribution for the slow (2–3 year) propagation of SSTA across the subtropical North Pacific is difficult with only the use of observational data, and further investigation is needed.

4.3 Role of the Indian Ocean basin

The interannual equatorial zonal wind stress across both the Indian Ocean and the equatorial Pacific are able to sustain the ENSO cycle. For instance, (Yu et al. 2002) have emphasized the impact of the Indian Ocean SSTA and wind processes on sustaining the ENSO cycle. These observations and the predominant 4–5 year frequency are suggestive of a hemispheric-scale atmospheric variability (at least over the Indian and Pacific Oceans) that acts to "regulate" the ENSO cycle. Whether or not the observed eastward migration revealed from the ocean heat content adjustment is triggered by such atmospheric forcing, or is it that the slow-changing ocean heat content modulates the atmospheric variability (like the NPO), remains. There is also a possibility that the ocean heat content migration as shown in Fig. 4 could feedback and produce the seemingly propagation of SSTA and atmospheric winds.

To fully understand the physical processes and uncover the mechanisms of the reported global-scale propagation

will require comprehensive modeling experiments. Doing so is beyond the scope of this study, yet our preliminary testing using the CMIP5-class models did suggest that some models are capable of simulating the 4–5-year frequency of ENSO and associated propagation patterns in both SSTA and SLP, as exemplified in Fig. 9. Further sensitivity experiments using those models will be the next task. Presently, the results from this study do imply that proper monitoring of the eastward migration of SSTA and the WNP pattern could assist in long-lead prediction of ENSO.

Acknowledgments Useful discussions with Michelle L'Heureux and TC Chen are highly appreciated. This study was supported by the NASA Grant NNX13AC37G and by the United States Agency for International Development Grant EEM-A-00-38310-00001.

References

Alexander MA, Vimont DJ, Chang P, Scott JD (2010) The impact of extratropical atmospheric variability on ENSO: testing the seasonal footprinting mechanism using coupled model experiments. J Clim 23(11):2885–2901

Anderson BT (2003) Tropical Pacific sea surface temperatures and preceding sea level pressure anomalies in the subtropical North Pacific. J Geophys Res 108(D23). doi:10.1029/2003JD003805

Barnett T (1983) Interaction of the monsoon and Pacific trade wind system at interannual time scales part I: the equatorial zone. Mon Wea Rev 111(4):756–773

Behringer DW, Ji M, Leetmaa A (1998) An improved coupled model for ENSO prediction and implications for ocean initialization part I: the ocean data assimilation system. Mon Wea Rev 126(4):1013–1021

Bejarano L, Jin F-F (2008) Coexistence of equatorial coupled modes of ENSO*. J Clim 21(12):3051–3067

Cayan DR (1992) Latent and sensible heat flux anomalies over the Northern Oceans: the connection to monthly atmospheric circulation. J Clim 5(4):354–369

Chang P, Zhang L, Saravanan R, Vimont DJ, Chiang JC, Ji L, Seidel H, Tippett MK (2007) Pacific meridional mode and El Nino-Southern oscillation. Geophys Res Lett 34(16):L16608

Chiang JCH, Vimont DJ (2004) Analogous Pacific and Atlantic Meridional modes of tropical atmosphere–ocean variability. J Clim 17(21):4143–4158

Chowdary JS, Xie S-P, Luo J-J, Hafner J, Behera S, Masumoto Y, Yamagata T (2011) Predictability of Northwest Pacific climate during summer and the role of the tropical Indian Ocean. Clim Dyn 36(3–4):607–621

Chowdary JS, Xie S-P, Tokinaga H, Okumura YM, Kubota H, Johnson N, Zheng X-T (2012) Interdecadal variations in ENSO teleconnection to the Indo-Western Pacific for 1870–2007*. J Clim 25(5):1722–1744

Clarke AJ (2008) An introduction to the dynamics of El Nino and the Southern oscillation. Academic Press, London, p 308

Clarke AJ, Van Gorder S (2003) Improving El Niño prediction using a space-time integration of Indo-Pacific winds and equatorial Pacific upper ocean heat content. Geophys Res Lett 30(7):1399

Clarke AJ, Liu X, Van Gorder S (1998) Dynamics of the biennial oscillation in the equatorial Indian and far western Pacific Oceans. J Clim 11(5):987–1001

Dickey JO, Marcus SL, de Viron O (2003) Coherent interannual and decadal variations in the atmosphere–ocean system. Geophys Res Lett 30(11):1573

Du Y, Yang L, Xie S-P (2011) Tropical Indian Ocean influence on Northwest Pacific tropical cyclones in summer following strong El Niño*. J Clim 24(1):315–322

Enfield DB, Mayer DA (1997) Tropical Atlantic sea surface temperature variability and its relation to El Niño-Southern oscillation. J Geophys Res Ocean (1978–2012) 102(C1):929–945

Gutzler DS, Harrison D (1987) The structure and evolution of seasonal wind anomalies over the near-equatorial eastern Indian and western Pacific Oceans. Mon Wea Rev 115(1):169–192

Hendon HH (2003) Indonesian rainfall variability: impacts of ENSO and local air–sea interaction. J Clim 16(11):1775–1790

Huang G, Hu K, Xie S-P (2010) Strengthening of tropical Indian Ocean teleconnection to the Northwest Pacific since the mid-1970s: an atmospheric GCM study*. J Clim 23(19):5294–5304

Huang W-R, Chen T-C, Wang S-Y (2012) Co-variability of poleward propagating atmospheric energy with tropical and higher-latitude climate oscillations. Clim Dyn 39(7–8):1905–1912

Iacobucci A, Noullez A (2005) A frequency selective filter for short-length time series. Comput Econ 25:75–102

Izumo T, Vialard J, Lengaigne M, de Boyer Montegut C, Behera SK, Luo J-J, Cravatte S, Masson S, Yamagata T (2010) Influence of the state of the Indian Ocean dipole on the following year's El Nino. Nat Geosci 3(3):168–172

Jin FF, An SI (1999) Thermocline and zonal advective feedbacks within the equatorial ocean recharge oscillator model for ENSO. Geophys Res Lett 26(19):2989–2992

Kalnay E et al (1996) The NCEP/NCAR 40-year reanalysis project. Bull Am Meteor Soc 77(3):437–471

Klein SA, Soden BJ, Lau N-C (1999) Remote sea surface temperature variations during ENSO: evidence for a tropical atmospheric bridge. J Clim 12(4):917–932

Lin H, Derome J, Greatbatch RJ, Andrew Peterson K, Lu J (2002) Tropical links of the Arctic oscillation. Geophys Res Lett 29(20):1943

Linkin ME, Nigam S (2008) The north pacific oscillation-west Pacific teleconnection pattern: mature-phase structure and winter impacts. J Clim 21(9):1979–1997

Mann M, Park J (1996) Greenhouse warming and changes in the seasonal cycle of temperature: model versus observations. Geophys Res Lett 23(10):1111–1114

McPhaden MJ (1999a) El Nino: the child prodigy of 1997–98. Nature 398(6728):559–562

McPhaden MJ (1999b) Genesis and evolution of the 1997–98 El Niño. Science 283(5404):950–954

Meehl GA (1987) The annual cycle and interannual variability in the tropical Pacific and Indian Ocean regions. Mon Wea Rev 115(1):27–50

Meyers G, McIntosh P, Pigot L, Pook M (2007) The years of El Niño, La Niña, and interactions with the tropical Indian Ocean. J Clim 20(13):2872–2880

Neelin JD, Battisti DS, Hirst AC, Jin FF, Wakata Y, Yamagata T, Zebiak SE (1998) ENSO theory. J Geophys Res Ocean (1978–2012) 103(C7):14261–14290

Penland C, Sardeshmukh PD (1995) The optimal growth of tropical sea surface temperature anomalies. J Clim 8(8):1999–2024

Rodríguez-Fonseca B, Polo I, García-Serrano J, Losada T, Mohino E, Mechoso CR, Kucharski F (2009) Are Atlantic Niños enhancing Pacific ENSO events in recent decades? Geophys Res Lett 36(20):L20705

Rogers JC (1981) The North Pacific oscillation. J Climatol 1(1):39–57

Smith TM, Reynolds RW, Peterson TC, Lawrimore J (2008) Improvements to NOAA's historical merged land–ocean surface temperature analysis (1880–2006). J Clim 21(10):2283–2296

Takayabu YN, Iguchi T, Kachi M, Shibata A, Kanzawa H (1999) Abrupt termination of the 1997–98 El Nino in response to a Madden–Julian oscillation. Nature 402(6759):279–282

Taylor KE, Stouffer RJ, Meehl GA (2011) An overview of CMIP5 and the experiment design. Bull Am Meteor Soc 93(4):485–498

Tourre YM, White WB (1997) Evolution of the ENSO signal over the Indo-Pacific domain*. J Phys Oceanogr 27(5):683–696

Vialard J, Menkes C, Boulanger J-P, Delecluse P, Guilyardi E, McPhaden MJ, Madec G (2001) A model study of oceanic mechanisms affecting equatorial Pacific sea surface temperature during the 1997–98 El Niño. J Phys Oceanogr 31(7):1649–1675

Vimont DJ, Battisti DS, Hirst AC (2001) Footprinting: a seasonal connection between the tropics and mid-latitudes. Geophys Res Lett 28(20):3923–3926

Vimont DJ, Wallace JM, Battisti DS (2003) The seasonal footprinting mechanism in the Pacific: implications for ENSO. J Clim 16(16):2668–2675

Walker GT, Bliss EW (1932) World weather V. Mem Roy Meteor Soc 4:53–84

Wallace JM, Gutzler DS (1981) Teleconnections in the geopotential height field during the Northern Hemisphere winter. Mon Wea Rev 109(4):784–812

Wang B, Wu R, Fu X (2000) Pacific-East Asian teleconnection: how does ENSO affect East Asian climate? J Clim 13(9):1517–1536

Wang L, Chen W, Huang R (2007) Changes in the variability of North Pacific oscillation around 1975/1976 and its relationship with East Asian winter climate. J Geophys Res Atmos 112(D11):D11110

Wang S-Y, L'Heureux M, Chia H-H (2012) ENSO prediction one year in advance using western North Pacific sea surface temperatures. Geophys Res Lett 39(5):L05702

Wang S-Y, L'Heureux M, Yoon J-H (2013) Are greenhouse gases changing ENSO precursors in the Western North Pacific? J Clim 26:6309–6322

White WB, Tourre YM, Barlow M, Dettinger M (2003) A delayed action oscillator shared by biennial, interannual, and decadal signals in the Pacific Basin. J Geophys Res 108(C3):1511–1518

Xie S-P, Annamalai H, Schott FA, McCreary JP Jr (2002) Structure and mechanisms of south Indian Ocean climate variability*. J Clim 15(8):864–878

Xie S-P, Hu K, Hafner J, Tokinaga H, Du Y, Huang G, Sampe T (2009) Indian Ocean capacitor effect on Indo-Western Pacific climate during the summer following El Niño. J Clim 22(3):730–747

Xie S-P, Du Y, Huang G, Zheng X-T, Tokinaga H, Hu K, Liu Q (2010) Decadal shift in El Niño influences on Indo-Western Pacific and East Asian climate in the 1970s*. J Clim 23(12):3352–3368

Yang J, Liu Q, Xie S-P, Liu Z, Wu L (2007) Impact of the Indian Ocean SST basin mode on the Asian summer monsoon. Geophys Res Lett 34(2):L02708

Yu J-Y, Mechoso CR, McWilliams JC, Arakawa A (2002) Impacts of the Indian Ocean on the ENSO cycle. Geophys Res Lett 29(8):4641–4644